Appl. Phys. B 73, 157–163 (2001) / Digital Object Identifier (DOI) 10.1007/s003400100621

Applied Physics B
Lasers
and Optics

Modifications to the lidar equation due to nonlinear propagation in air

G. Faye*, J. Kasparian, R. Sauerbrey

Institut für Optik und Quantenelektronik, Friedrich Schiller Universität Jena, Max Wien Platz 1, 07743 Jena, Germany

Received: 2 January 2001/Revised version: 8 June 2001/Published online: 18 July 2001 –

Abstract. We study how the well-known lidar equation is affected by the use of ultra-short, high-power laser pulses. Because of the self-focusing and self-guiding, the overlap function ξ, representing the reduction fraction of the signal resulting from geometrical effects inside the experimental system, needs to be reconsidered. The losses due to multiphoton ionisation in the filament entail a heavy weakening of the return signal. We also investigate the contribution of the white-light components generated by self-phase modulation.

PACS: 42.50.H; 42.68; 42.65.R; 42.68.W

Light detection of ranging (lidar) [1, 2], an optical analogue of radar, is now a classical technique for atmospheric remote sensing, with unique versatility and three-dimensional (3D) mapping abilities. However, retrieving the atmospheric composition from a lidar signal is not straightforward. Gases with narrow absorption lines may be detected by the Differential Absorption Lidar (DIAL) technique. For gases with overlapping absorption bands leading to interference in the measurements, or for aerosols [3], strong assumptions regarding the particles at play are necessary in order to determine absolute concentrations.

Recently, it has been proposed [4] and demonstrated [5, 6] that nonlinear lidar measurements based on high-power femtosecond laser pulses could provide more information than their linear counterparts. A white-light supercontinuum generated by high-power laser pulses propagating in air provides a broadband pulsed light source from the ultraviolet (UV) [7] to the infrared (IR) [8]. The IR wavelengths, which have been measured up to 4.5 μm, open the way to measurements of pollutants absorbing in this spectral domain such as methane, or with overlapping spectra, such as volatile organic compounds, which could be resolved through multi-spectral lidar measurements [5]. A white light supercontinuum lidar signal was observed up to 13 km [5, 6]. Ultra-short pulses could also give rise to significant size effects in the microcavities formed by spherical, transparent aerosols such as cloud droplets. When the pulse is shorter than the cavity length, it can be localised in the aerosol cavity. This so-called ballistic mode may lead to a strong enhancement of the lidar signal received from the smallest particles [4, 25].

Nonlinear lidar requires high-power, ultra-short (femtosecond) laser pulses which have a very complex behaviour when propagating in air. Basically, they first undergo self-focusing due to the Kerr effect, giving rise to a sharp increase in the intensity. Then, ionisation takes place and induces defocusing. The equilibrium between these two processes leads to a self-guided filament [9–12] with a diameter of about 100 μm, and which can expand over distances of at least 200 m [13]. Due to the high intensities in the filament, a strong self-phase modulation occurs, which entails a wide spectral broadening, i.e. the supercontinuum generation mentioned above.

On the other hand, losses due to the ionisation in the filament lead to a decrease of the pulse energy. When this intensity has fallen below a critical value [24], the balance between Kerr focusing and plasma defocusing can no longer be maintained and the self-focused filament ends. Then the beam undergoes a so-called conical emission [10, 14, 15] with a typical divergence of 0.1°. The precise mechanism of the filament propagation is not yet clear. At least three models have been proposed: moving focus [11], the self-wave-guiding model [9, 10] and the spatial replenishment model [12]. Analytical [16–18] as well as numerical [19–23] computations simulating the propagation of high-power laser pulses in air are difficult because of the high nonlinearity of the processes at play. This leads to typical computing times of 1 h per calculated metre of propagation, which would correspond to 1 year for a 10-km path. Such values illustrate the need for a more phenomenological description allowing a numerical treatment of the propagation of high-power laser pulses over the several-kilometre ranges involved in lidar experiments, and hence for a computationally efficient nonlinear lidar equation.

The first nonlinear extension to the lidar equation was proposed by Kasparian and Wolf [4]. However, this work focused mainly on the changes to the backscattering term due to transient size effects in aerosols. Propagation effects such as self-focusing were not considered there; hence the extinction term

*Corresponding author.
(Fax: +49-3641/947-102, E-mail: g.faye@tpi.uni-jena.de)

was left unchanged, which is physically unrealistic in view of the high power at play. In this Letter, we investigate the modifications to the geometrical and propagation/extinction terms due to nonlinear propagation of high-power laser beams, assuming an idealised shape.

At this stage, it is worth recalling the usual linear lidar equation [1]. The detected power E collected by a detector with surface A_0 after the backscattering of a laser beam of initial power E_L and wavelength λ_0 is given by

$$E(\lambda_0, z) = E_\mathrm{L} \frac{A_0}{z^2} \frac{c\tau_\mathrm{d}}{2} \xi(\lambda_0, z) \times \beta(\lambda_0, z) \exp\left(-2 \int_0^z \alpha_\ell(\lambda_0, z')\mathrm{d}z'\right) . \quad (1)$$

Here, z denotes the distance from the detector to the atmosphere slice where the light backscatters; α_ℓ and β are the extinction and the backscattering coefficients respectively. The overlap function $0 \leq \xi(\lambda_0, z) \leq 1$ includes the various signal losses due to the specific geometrical configuration of the system laser/detector. As for τ_d and c, they are respectively the length of the pulse and the speed of light in air. The meaning of the different contributions in (1) is rather clear. A part of the laser power E_L is absorbed or scattered according to the Beer–Lambert (exponential) law during the forward travel. Then, a part $\beta A_0/z^2$ of the power available at distance z is re-emitted back to the detector, and exponentially attenuated again (hence the factor 2 in front of α_ℓ) before reaching the telescope. The appearance of the factor $c\tau_\mathrm{d}/2$ is related to the fact that the power recovered immediately after the backscattering is proportional to the thickness of the atmospheric slice coming into play.

In the present paper, we shall modify the standard lidar equation (1) in order to describe both geometrical beam-shape influence (Sect. 1) and extinction due to multi-photon ionisation (Sect. 2), which are the two main effects at play in the propagation of high-power laser pulses. From this, we shall deduce an approximate expression for the signal produced by the individual spectral components of the white light (Sect. 3). As for the geometrical effect, our assumptions are as follows: after self-focusing at a distance z_f from the source, the laser beam gives rise to a filament of length z_fil that spreads out along the first tens or hundreds of metres and, finally, diverges like a spherical wave (conical emission). As a first approximation, we consider that this filament is a cylinder of diameter $2a \sim 100\,\mu\mathrm{m}$ [9]. On the other hand, following [15], we assume that, after diverging, the beam actually becomes a cone with half top angle $\theta_\mathrm{CE} \sim 0.1°$. From the previous hypothesis, we evaluate the factor ξ in the case where it is solely due to the default of overlap with the viewing cone of the detector, neglecting in particular the specific features coming from the design of the telescope. In our notation, θ_T represents the half opening angle of the telescope field of view, and ψ the possible deviation of its axis from the laser direction. The horizontal separation between both devices is denoted by D (see Fig. 1). In the following, we shall always suppose that ψ is positive or null (i.e. the telescope is either parallel to or inclined towards the laser beam), and that θ_CE, as well as θ_T, are (strictly) positive.

In order to evaluate the overall extinction term, we assume that during the back-travel of light, the intensity of the beam is sufficiently small so that we can neglect the nonlinear effects, and consider that only the forward-beam propagation is submitted to a nonlinear absorption regime resulting from multi-photon ionisation (which entails extra losses). The corresponding term in the local energy balance equation is proportional to a certain power $n > 1$ of intensity I, thus depending on the cross-section (and therefore the shape) of the beam. Notice that the pulse attenuation due to other mechanisms such as spectral broadening are neglected here. This is supported notably by spectral measurements of the supercontinuum [8], which exhibit no significant energy loss caused by the continuum-generation process, and show a steep decrease of the spectrum on both sides of the fundamental wavelength.

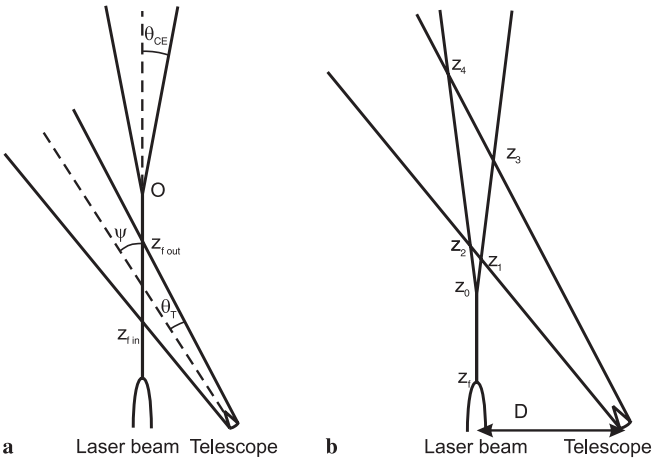

Fig. 1a,b. Two possible geometries of the relative positions of the telescope field of view and the laser beam: **a** the telescope sees only a section of the filament, as detailed in case (3) in the text; **b** the telescope intercepts only a part of the conical emission (case (1) in the text)

1 Geometrical effects

We first consider the fact that nonlinearity gives rise to a change in the shape of the laser beam, which leads to a modification in the overlap function ξ. It is easy to convince oneself that this represents merely the fraction of the beam cross-section, with radius $R_\mathrm{L}(z)$ at a distance z, intersecting the viewing cone of the telescope. Provided ψ does not exceed a few degrees, the horizontal section of the viewing cone is nearly circular, with radius R_T, and the problem amounts to computing the overlap area $\mathcal{A}(R_\mathrm{L}, R_\mathrm{T}, d)$ of two coplanar disks, with radii R_L and R_T, having their centres located at a distance d from each other (as represented in Fig. 2). If $(R_\mathrm{L} + R_\mathrm{T}) \leq d$, the disks have at most one point in common and $\mathcal{A}(R_\mathrm{L}, R_\mathrm{T}, d)$ reduces to zero. As soon as the circles are secant, $\mathcal{A}(R_\mathrm{L}, R_\mathrm{T}, d)$ is given by

$$\begin{aligned}\mathcal{A}(R_\mathrm{L}, R_\mathrm{T}, d) &= f(R_\mathrm{L}, R_\mathrm{T}, d) \\ &\equiv {R_\mathrm{L}}^2 \arccos\left(\frac{a_\mathrm{L}}{R_\mathrm{L}}\right) - a_\mathrm{L}\sqrt{{R_\mathrm{L}}^2 - {a_\mathrm{L}}^2} \\ &\quad + {R_\mathrm{T}}^2 \arccos\left(\frac{a_\mathrm{T}}{R_\mathrm{T}}\right) - a_\mathrm{T}\sqrt{{R_\mathrm{T}}^2 - {a_\mathrm{T}}^2}\,, \quad (2)\end{aligned}$$

where the auxiliary length $a_\mathrm{L} = (d^2 + {R_\mathrm{L}}^2 - {R_\mathrm{T}}^2)/(2d)$ measures the algebraic distance between the centre of the first

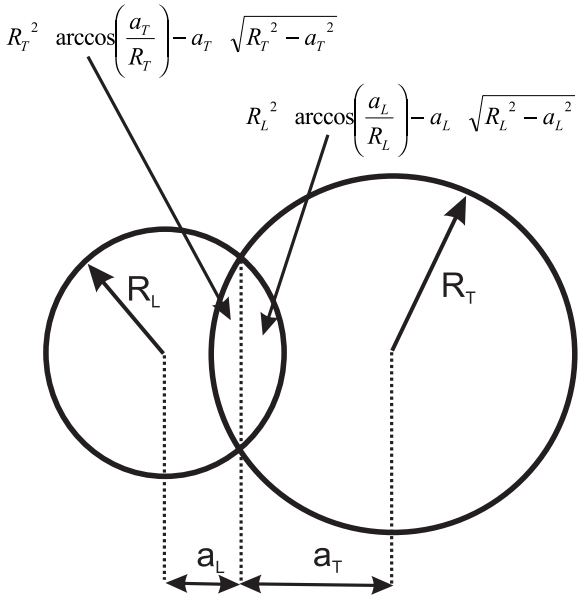

Fig. 2. Two secant circles with radii $R_{\rm L}$, $R_{\rm T}$; $a_{\rm L}$ and $a_{\rm T}$ are the same distances as defined in the text; the central overlap region is split into two parts by the string joining the intersecting points; the *arrows* indicate their respective areas

circle (with radius $R_{\rm L}$) and the string joining the two intersecting points (see Fig. 2); it is actually a function of the three variables d, $R_{\rm L}$ and $R_{\rm T}$. The definition of $a_{\rm T}$ is similar with the role of $R_{\rm L}$ and $R_{\rm T}$ exchanged, hence $a_{\rm T} = d - a_{\rm L} = (d^2 + {R_{\rm T}}^2 - {R_{\rm L}}^2)/(2d)$. Finally, when one of the disks contains the other one, i.e. $|R_{\rm L} - R_{\rm T}| \geq d$, then $\mathcal{A}(R_{\rm L}, R_{\rm T}, d) = \min(\pi {R_{\rm L}}^2, \pi {R_{\rm T}}^2)$.

All what we need now for getting $\xi_{\rm NL} \equiv \mathcal{A}(R_{\rm L}, R_{\rm T}, d)/(\pi {R_{\rm L}}^2)$ is to replace $R_{\rm L}$, $R_{\rm T}$ and d in the expression of $\xi_{\rm NL}$ by their actual values, in view of the geometrical configuration of our system. Since the angles $\theta_{\rm T}$, $\theta_{\rm CE}$ and ψ have small values (typically less than a few degrees), it is not worth working beyond the first order in any of these quantities. We shall write:

$$R_{\rm T} \approx z\theta_{\rm T}\,, \qquad d \approx |D - z\psi|\,. \tag{3}$$

The expression of $R_{\rm L}$ as a function of z depends on whether $z \leq z_{\rm f}$, $z_{\rm f} \leq z \leq z_{\rm fil}$ or $z_{\rm fil} \leq z$ (three segments). The shortest distances are of little interest in lidar measurements; moreover, in this range, the geometry of the telescope has a strong influence on the overlap function. Hence, we will not consider them in the following, and assume that $\xi_{\rm NL}(z) = 0$ for $z \leq z_{\rm f}$. Moreover, the radius a of the filament is indeed much smaller than the length $z_0 = z_{\rm f} + z_{\rm fil}$ and can be taken to be zero. Therefore, $R_{\rm L} = a \approx 0$ in the filament ($z \leq z_0$). Above it, $R_{\rm L} \approx (z - z_0)\theta_{\rm CE}$. Now, the function f can be viewed as a function of z only, and more precisely we shall define $\tilde{f}(z) = f((z - z_0)\theta_{\rm CE}, z\theta_{\rm T}, |D - z\psi|)$.

Like the radius $R_{\rm L}$, the overlap function has to be derived by segment. In the filament, it is convenient to define two particular distances $z_{\rm fin} = D/(\psi + \theta_{\rm T})$ and $z_{\rm fout} = D/(\psi - \theta_{\rm T})$, where the filament enters and exits the viewing cone of the telescope (see Fig. 1). Clearly, those distances can have a meaning only if they are below the end of the filament, i.e.provided $z_{\rm fin} \leq z_{\rm fout} \leq z_0$. Then, in the altitude range corresponding to the filament, we have $\xi_{\rm NL}(z) = 1$ for $z_{\rm fin} \leq z \leq \max(z_{\rm fout}, z_0)$ and $\xi_{\rm NL}(z) = 0$ everywhere else. After the conical emission ($z \geq z_0$), more geometrical combinations can occur, leading to more cases.

To go further in the study of these different cases, we introduce the altitudes of the four intersection points between the conical emission and the viewing cone of the telescope, as shown in Fig. 1: $z_1 = (D + z_0\theta_{\rm CE})/(\psi + \theta_{\rm T} + \theta_{\rm CE})$, $z_2 = (D - z_0\theta_{\rm CE})/(\psi + \theta_{\rm T} - \theta_{\rm CE})$, $z_3 = (D + z_0\theta_{\rm CE})/(\psi - \theta_{\rm T} + \theta_{\rm CE})$ and $z_4 = (D - z_0\theta_{\rm CE})/(\psi - \theta_{\rm T} - \theta_{\rm CE})$. Again, those definitions only make sense when the corresponding points are above z_0. Values less than z_0 lead to no crossing points. In that case, they can be cast to $+\infty$ for our discussion.

We have to distinguish between three cases.

1. If $z_1 \geq z_0$ (or equivalently if $z_{\rm fin} \geq z_0$) then the field of view of the telescope intersects only with the conical emission; it is always the case for linear lidar, where results can be obtained from the above discussion by choosing $z_0 = 0$.
   (a) under ($z \leq z_1$) or above ($z \geq z_4 \geq z_0$) the field of view of the telescope, we have $\xi_{\rm NL}(z) = 0$;
   (b) if $z_0 \leq z_2 \leq z \leq z_3$, the laser beam is included in the field of view of the telescope and $\xi_{\rm NL}(z) = 1$;
   (c) if $z_0 \leq z_3 \leq z \leq z_2$, then the field of view of the telescope is included in the laser beam, so that $\xi_{\rm NL}(z) = [z\theta_{\rm T}/((z - z_0)\theta_{\rm CE})]^2$;
   (d) everywhere else, i.e. for $z_1 \leq z \leq \min(z_2, z_3)$ or for $\max(z_2, z_3) \leq z \leq z_4$ (remember that z_4 is taken to be $+\infty$ if $z_4 \leq z_0$), the two cones cross each other; hence $\xi_{\rm NL}(z) = \tilde{f}(z)$.

2. If $z_{\rm fin} \leq z_0 \leq z_{\rm fout}$ (which implies that $z_1 \leq z_0$), then the field of view of the telescope includes the point O where the beam starts diverging. In this second case:
   (a) under ($z \leq z_{\rm fin}$) or above ($z \geq z_4 \geq z_0$) the field of view of the telescope, we have $\xi_{\rm NL}(z) = 0$;
   (b) if $z_{\rm fin} \leq z \leq \min(z_2, z_3)$, the laser beam is included in the field of view of the telescope and $\xi_{\rm NL}(z) = 1$;
   (c) Above $\max(z_2, z_3) \geq z_0$, the field of view of the telescope remains inside the laser beam and $\xi_{\rm NL}(z) = [z\theta_{\rm T}/((z - z_0)\theta_{\rm CE})]^2$;
   (d) If $\min(z_2, z_3) \leq z \leq \min(\max(z_2, z_3), z_4)$, then the overlap function is given by $\xi_{\rm NL}(z) = \tilde{f}(z)$;

   In the two latter cases, one has again to keep in mind the convention that any z_i smaller than z_0 must equal $+\infty$.

3. If $z_{\rm fin} \leq z_{\rm fout} \leq z_0$, the viewing cone completely crosses the filament under the point O. However, it may intersect afterwards with the conical emission, provided $z_4 \geq z_0$. Again, four sub-cases have to be distinguished:
   (a) under the intersection with the field of view of the telescope ($z \leq z_{\rm fin}$) and over this intersection up to the possible intersection with the conical emission ($z_{\rm fout} \leq z \leq z_4$), we have $\xi_{\rm NL}(z) = 0$;
   (b) in the section of the filament that is intercepted by the telescope field of view ($z_{\rm fin} \leq z \leq z_{\rm fout}$), we have $\xi_{\rm NL}(z) = 1$;
   (c) for $z \geq z_2 \geq z_0$, the field of view of the telescope completely enters the conical emission and $\xi_{\rm NL}(z) = [z\theta_{\rm T}/((z - z_0)\theta_{\rm CE})]^2$;

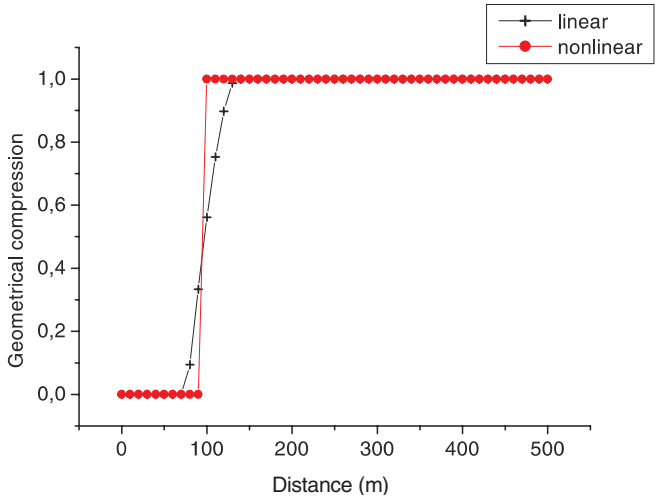

Fig. 3. Overlap function $\xi_{\mathrm{NL}}(z)$ (*thick points*) in the case where the viewing cone contains a part of the filament and the whole conical emission; $D = 0.33\,\mathrm{m}$; $z_{\mathrm{f}} = 1.00\,\mathrm{m}$; $z_{\mathrm{fil}} = 100\,\mathrm{m}$; $\psi = 1 \times 10^{-3}$; $\theta_{\mathrm{T}} = 2.5 \times 10^{-3}$; $\theta_{\mathrm{CE}} = 1 \times 10^{-3}$. Compare to the standard situation for $z_0 = 0\,\mathrm{m}$ (*crosses*)

(d) for $z_4 \leq z \leq z_2$ (with, again, z_2 equal to $+\infty$ if $z_2 < z_0$), the field of view of the telescope intersects the conical emission, hence $\xi_{\mathrm{NL}}(z) = \tilde{f}(z)$.

The complication of the result is only apparent, and comes from the high number of geometrical configurations occurring in each case, according to the relative values of the various angles. However, given a specific set of parameters, the function $\xi_{\mathrm{NL}}(z)$ takes a very simple form. Note that when the cone of view contains a part of the filament as well as the whole conical emission, $\xi_{\mathrm{NL}}(z)$ jumps abruptly from 0 to 1, and then remains constant (see the 'step' in Fig. 3). This leads to a much simpler overlap function than for the linear case, where $\xi_{\mathrm{NL}}(z)$ rises more slowly from 0 to 1. However, when the cone of view of the telescope intersects with the laser beam above the filament, the geometrical term becomes quite similar to that of the linear case, with only an offset z_0 in the distance z and both expressions even coincide for $z_0 = 0$. In this respect, all the nonlinear effects arise through the filament length, which is actually an implicit (unspecified) function of initial intensity $z_0 = z_0(I_0)$; $z_0(I_0)$ goes to zero when I_0 becomes small enough, since we must then come back to the linear regime.

2 Effect of the nonlinear absorption

Apart from modifying the overlap function ξ_{NL}, as already mentioned, the main nonlinear corrections to the lidar equation affect the exponential extinction factor in (1). Indeed, during the forward travel when the intensity is extremely high, a part of the energy of the laser pulse is used to ionise the atmosphere, and the absorption due to multi-photon ionisation losses adds up to the usual linear (Mie and Raleigh) scattering. If n represents the number of photons that are necessary to ionise one molecule, the corresponding intensity losses (for a plane wave) read

$$\left(\frac{\mathrm{d}I}{\mathrm{d}z}\right)_{\mathrm{MPI}} = \alpha_{\mathrm{ref}} \left(\frac{I}{I_{\mathrm{ref}}}\right)^n , \tag{4}$$

with $\alpha_{\mathrm{ref}} = nh\nu_{\mathrm{L}} R_{\mathrm{ref}} N$, where $h\nu_{\mathrm{L}}$ is the laser photon energy, N the ionising molecule density and R_{ref} a reference ionisation rate of the considered species, which has to be determined experimentally as does the reference intensity I_{ref} [24]. As a matter of fact, the values of n are given by experiment, and are rather effective values taking all ionisation processes into account. In particular, tunnel ionisation may lead to fractional values lower than those expected from the ratio of the ionisation potential to the photon energy. As the number n differs from one type of ionised molecule to another, the complete losses are made up of a sum of terms such as the one given by (4) with various values for α_{ref}, I_{ref} and n. However, provided the intensity remains below $10^{18}\,\mathrm{W/m^2}$, the contribution of oxygen dominates in air [24], so that we are allowed to keep only one term in the sum as a first approximation. Higher intensities would moreover produce the saturation of ionisation and alter (4). Besides, our assumption leads us to an analytical solution for the intensity, which provides quite a realistic description of the main changes induced by nonlinearity.

Now, a laser beam can be seen as a divergent wave, emitted by a fictitious point O in a cone of solid angle Ω. The energy-density variation in the spherical slice of centre O, radius r ($\approx z$ in our case) and thickness dr is assumed to be entirely due to scattering or absorption. We look for I as a function of r only, hence the balance equation:

$$\begin{aligned} &I(r+\mathrm{d}r)\,(r+\mathrm{d}r)^2\Omega - I(r)r^2\Omega = \\ &-\alpha_\ell(r)\,I r^2 \mathrm{d}r\Omega - \alpha_{\mathrm{ref}}(r)\left(\frac{I}{I_{\mathrm{ref}}}\right)^n r^2 \mathrm{d}r\Omega\,, \end{aligned} \tag{5}$$

where α_ℓ denotes the linear scattering coefficient. The differential equation obeyed by the intensity function then reads:

$$\frac{\mathrm{d}I}{\mathrm{d}r} = -\frac{2}{r}I - \alpha_\ell I - \alpha_{\mathrm{ref}}\left(\frac{I}{I_{\mathrm{ref}}}\right)^n , \tag{6}$$

where we immediately recognise a Bernoulli equation. The solution is readily obtained by introducing the intermediate unknown function $y(r) = I^{1-n}(r)$. We find after easy calculations

$$\begin{aligned} I(r) = I_0 \left(\frac{r_0}{r}\right)^2 &\exp\left(-\int_{r_0}^{r} \alpha_\ell(\lambda_0, r')\mathrm{d}r'\right) \\ &\times \left[1 + (n-1)\left(\frac{{r_0}^2 I_0}{I_{\mathrm{ref}}}\right)^{n-1} \int_{r_0}^{r} \varrho^{-2(n-1)} \left(\frac{\alpha_{\mathrm{ref}}(\varrho)}{I_{\mathrm{ref}}}\right) \right. \\ &\left. \times \exp\left(-(n-1)\int_{r_0}^{\varrho} \alpha_\ell(\lambda_0, \varrho')\mathrm{d}\varrho'\right) \mathrm{d}\varrho \right]^{-1/(n-1)} . \end{aligned} \tag{7}$$

The parameter I_0 can be interpreted as the intensity of the beam at a distance $r = r_0$ from the point O. The solution $I(r)$ behaves as $1/r^2$ when r goes to zero and, therefore, it represents the propagation of a spherical wave outward from the source. The first exponential factor is mainly responsible for the energy decrease for large values of α_ℓ in agreement with

the Beer–Lambert law. The new feature comes from the contribution appearing between the square brackets. The second term inside the brackets represents the correction due to nonlinear absorption during the propagation process. It can be seen as resulting from the multi-photon ionisation (4) applied to the linearly attenuated beam. It is of course negligible when the intensity of the beam I becomes small with respect to the reference intensity I_{ref}, but at the exit of the laser, we may have $I \gg I_{\mathrm{ref}}$ if the initial power E_{L} is high enough, so that the ionisation effect dominates. On the other hand, at short distance, i.e. for $r \ll 1/\alpha_\ell$, the exponential factor modulating the integrand $\varrho^{-2(n-1)}\alpha_{\mathrm{ref}}(\varrho)/I_{\mathrm{ref}}$ as well as the one of the Beer–Lambert extinction are close to 1. In summary, we can distinguish between three different absorption regimes provided the initial power is sufficient: (i) for $r \ll 1/\alpha_\ell$ the absorption is dominated by multi-photon ionisation, (ii) for $r \gg 1/\alpha_\ell$ it obeys the Beer–Lambert law, (iii) for $r \sim 1/\alpha_\ell$ we have an intermediate regime where the full expression of the intensity should be used. Note that if we make n formally go to 1 in (7), the bracket tends towards an exponential function, which is not surprising, since then both energy-loss terms in the balance equation (5) are proportional to the intensity.

In the filament, the beam has to be treated as a plane wave (along the z axis). Starting from the energy-conservation equation

$$\frac{\mathrm{d}I}{\mathrm{d}z} = -\alpha_\ell I - \alpha_{\mathrm{ref}}\left(\frac{I}{I_{\mathrm{ref}}}\right)^n \tag{8}$$

and following the same method as the one sketched above, we get the alternative solution, valid for plane propagation:

$$\begin{aligned} I(z) = I_0 \exp\left(-\int_{Z_0}^{z} \alpha_\ell(\lambda_0, z')\mathrm{d}z'\right) \\ \times \left[1 + (n-1)\left(\frac{I_0}{I_{\mathrm{ref}}}\right)^{n-1} \int_{Z_0}^{z} \left(\frac{\alpha_{\mathrm{ref}}(\zeta)}{I_{\mathrm{ref}}}\right) \right. \\ \left. \times \exp\left(-(n-1)\int_{Z_0}^{\zeta} \alpha_\ell(\lambda_0, \zeta')\mathrm{d}\zeta'\right)\mathrm{d}\zeta\right]^{-1/(n-1)} . \end{aligned} \tag{9}$$

There are only a few changes with respect to the spherical-wave case: the factor $1/r^2$ has disappeared, and the source inside the integral over $\mathrm{d}\zeta$ has been modified by removing the singular factor $\varrho^{-2(n-1)}$ appearing in (7).

Combining both results, we obtain the intensity of the laser beam inside the filament as well as after the conical emission. Over the first centimetres or metres of the light travel, i.e. just before the self-focusing, the power losses are nearly negligible with respect to the total available energy per time unit E_{L}; thus, the power at the beginning of the filament $P(z_{\mathrm{f}}) \equiv \pi a^2 I(z_{\mathrm{f}})$ is almost equal to E_{L}. Now, the intensity of the laser as a function of z is given for $z \le z_0$ by the relation (9), where Z_0 is taken to be equal to z_{f} in order to have $I_0 = E_{\mathrm{L}}/(\pi a^2)$. This leads to a transmission coefficient in the filament

$$\begin{aligned} T_{\mathrm{NL}}(\lambda_0, I_0, z) = \exp\left(-\int_{z_{\mathrm{f}}}^{z} \alpha_\ell(\lambda_0, z')\mathrm{d}z'\right) \\ \times \left[1 + (n-1)\left(\frac{I_0}{I_{\mathrm{ref}}}\right)^{n-1} \int_{z_{\mathrm{f}}}^{z} \left(\frac{\alpha_{\mathrm{ref}}(\zeta)}{I_{\mathrm{ref}}}\right) \right. \\ \left. \times \exp\left(-(n-1)\int_{z_{\mathrm{f}}}^{\zeta} \alpha_\ell(\lambda_0, \zeta')\mathrm{d}\zeta'\right)\mathrm{d}\zeta\right]^{-1/(n-1)} , \end{aligned} \tag{10}$$

with the restriction $z \le z_0$. The intensity near the top of the emitting cone is then straightforwardly deduced from the value of the light power at the end of the filament: $P(z_0) = \pi a^2 I(z_0)$. If r_0 is a small arbitrary length as compared to z_0, say $r_0 \sim a/\theta_{\mathrm{CE}}$, there is very little absorption or backscattering between z_0 and $z_0 + r_0$, and we can write $\pi\theta_{\mathrm{CE}}{}^2 r_0{}^2 I(z_0 + r_0) \approx P(z_0)$. As a consequence, we determine the intensity $I(z)$ in the region of the conical emission by substituting $(a/\theta_{\mathrm{CE}})^2 I(z_0)$ with $r_0{}^2 I_0$ as well as $(z - z_0)$ with r in (7). We must also replace the backscattering coefficient $\alpha_\ell(\varrho)$ by $\alpha_\ell(z_0 + \varrho)$ (and the same for α_{ref}).

$$\begin{aligned} I(z) = I_0\left(\frac{a}{\theta_{\mathrm{CE}}(z - z_0)}\right)^2 \exp\left(-\int_{z_{\mathrm{f}}}^{z} \alpha_\ell(\lambda_0, r)\mathrm{d}r\right) \\ \times \left[1 + (n-1)\left(\frac{I_0}{I_{\mathrm{ref}}}\right)^{n-1} \int_{z_{\mathrm{f}}}^{z_0} \left(\frac{\alpha_{\mathrm{ref}}(\varrho)}{I_{\mathrm{ref}}}\right) \right. \\ \left. \times \exp\left(-(n-1)\int_{z_{\mathrm{f}}}^{\varrho} \alpha_\ell(\lambda_0, \varrho')\mathrm{d}\varrho'\right)\mathrm{d}\varrho \right. \\ \left. + (n-1)\left(\frac{a^2 I_0}{\theta_{\mathrm{CE}}{}^2 I_{\mathrm{ref}}}\right)^{n-1} \right. \\ \left. \times \exp\left(-(n-1)\int_{z_{\mathrm{f}}}^{z_0} \alpha_\ell(\lambda_0, r')\mathrm{d}r'\right) \right. \\ \left. \times \int_{z_0 + r_0}^{z} \frac{\alpha_{\mathrm{ref}}(\varrho)}{I_{\mathrm{ref}}(\varrho - z_0)^{2(n-1)}} \right. \\ \left. \times \exp\left(-(n-1)\int_{z_0}^{\varrho} \alpha_\ell(\lambda_0, \varrho')\mathrm{d}\varrho'\right)\mathrm{d}\varrho\right]^{-1/(n-1)} . \end{aligned} \tag{11}$$

The constant r_0 has been neglected everywhere except in the lower bound of the second integral over $\mathrm{d}\varrho$, which happens to diverge when r_0 goes to zero. Such a behaviour is not surprising, since in the case of a rigorously spherical wave, the intensity becomes infinite at the origin, which would imply a total nonlinear absorption in the framework of classical electromagnetism. Of course, this situation is not physical and, to a certain extent, the filament 'matches' the emitting cone. Setting $r_0 = a/\theta_{\mathrm{CE}}$ amounts to imposing the continuity of the section radius, but this choice is arbitrary. However, as soon as the diameter of the conical emission is significantly larger than that of the filament, the pre-factor of the

latter integral becomes negligible, and the numerical result should not be notably modified. Again, the first (exponential) factor accounts for linear extinction; the second term of the factor between brackets is associated with the multi-photon ionisation inside the filament, while the last term describes the multi-photon ionisation after the conical emission as obtained from (7) and (9). Neglecting the latter contribution, we define the transmission factor for $z \geq z_0$ (beyond the conical emission) as

$$T_{\mathrm{NL}}(\lambda_0, I_0, z) \equiv \left(\frac{\theta_{\mathrm{CE}}(z-z_0)}{a}\right)^2 \frac{I(z)}{I_0}$$
$$\approx \exp\left(-\int_{z_\mathrm{f}}^{z} \alpha_\ell(\lambda_0, r)\mathrm{d}r\right)\left[1+(n-1)\left(\frac{I_0}{I_{\mathrm{ref}}}\right)^{n-1}\right.$$
$$\left.\times\int_{z_\mathrm{f}}^{z_0}\left(\frac{\alpha_{\mathrm{ref}}(\varrho)}{I_{\mathrm{ref}}}\right)\exp\left(-(n-1)\int_{z_\mathrm{f}}^{\varrho}\alpha_\ell(\lambda_0,\varrho')\mathrm{d}\varrho'\right)\mathrm{d}\varrho\right]^{-1/(n-1)}. \tag{12}$$

To get the nonlinear lidar equation, it only remains to perform the replacement

$$\exp\left(-2\int_0^z \alpha_\ell(\lambda_0, z')\mathrm{d}z'\right) \rightarrow$$
$$\exp\left(-\int_0^z \alpha_\ell(\lambda_0, z')\mathrm{d}z'\right) T_{\mathrm{NL}}(\lambda_0, I_0, z) \tag{13}$$

in (1), remembering that $I_0 = E_\mathrm{L}/(\pi a^2)$, and using a suitable overlap factor. We finally arrive at

$$E(\lambda_0, z) = E_\mathrm{L}\frac{A_0}{z^2}\frac{c\tau_\mathrm{d}}{2}\xi_{\mathrm{NL}}(\lambda_0, I_0, z)$$
$$\times\beta(\lambda_0, z)\exp\left(-\int_0^z \alpha_\ell(\lambda_0, z')\mathrm{d}z'\right) T_{\mathrm{NL}}(\lambda_0, I_0, z), \tag{14}$$

where ξ_{NL} is that of Sect. 1 and T_{NL} is given by (10) or (12) depending on whether $z_\mathrm{f} \leq z \leq z_0$ or $z_0 \leq z$ respectively.

If we compare this nonlinear lidar equation with the linear one (1), it is clear that the effect of the pulse extinction due to multi-photon ionisation results in a heavy reduction (up to several orders of magnitude) of the available power at the end of the filament. However, in the diverging region, where the beam section is much larger, multi-photon ionisation is negligible and, thus, the distance-dependence of the lidar return is similar to that of the linear case. Of course, in the extreme situation where the intensity tends to zero, T_{NL} reduces to the Beer–Lambert absorption coefficient. As we also have $\xi_{\mathrm{NL}} \rightarrow \xi$ in this limit, we recover the linear lidar equation (1) for small values of I.

3 Multi-spectral lidar signal

Due to spectral broadening resulting from self-phase modulation, a nonlinear lidar offers a unique opportunity to perform multi-spectral experiments. In this purpose, we shall derive here the lidar signal produced at a wavelength λ different from the wavelength λ_0 of the laser.

If multiple scattering is neglected, there are two different ways for the white light to reach the detector at time $t = 2z/c$: (i) a direct backward emission at altitude z, which may be treated as in [4] (see (5) therein), with T_{NL} given by (12) above, or (ii) a forward white-light emission at a distance $z_{\mathrm{em}} \leq z$, followed by a backscattering at distance z. Recent measurements [26] suggest that the white-light energy is negligible outside the conical emission [10, 14, 15], i.e. we can consider that the white light is emitted forward in a cone with half top angle $\theta_{\mathrm{em}} \approx \theta_{\mathrm{CE}}$. The geometrical factor $\xi_{\mathrm{NL}}(\lambda, I_0, z_{\mathrm{em}}, z)$ thus has the same form as the one of Sect. 1 in the case $z \geq z_0$, but the role of z_0 is now held by z_{em}.

The white-light intensity travelling in the backward direction is small enough to consider its propagation as linear. In contrast, nonlinearities may affect the forward propagation via the influence of the co-propagating pump pulse. In that case, obtaining an analytical expression of the transmission factor for the white light is an extremely difficult task, due to the numerous processes to be taken into account. We shall neglect all effects of that kind in our simple model. Under this hypothesis, the extinction of forward-travelling (as well as backward-travelling) white light is correctly described by the Beer–Lambert law. If we denote by $\beta_{\mathrm{for}}(\lambda, \lambda_0, I_0, z_{\mathrm{em}})$ the conversion coefficient from wavelength λ_0 to wavelength λ, at distance z_{em} from the source with initial intensity I_0, the contribution to the intensity $\mathrm{d}I_{\mathrm{for}}(\lambda, I_0, z)$ at altitude z generated on a shell of thickness $\mathrm{d}z_{\mathrm{em}}$ at altitude z_{em} reads

$$\mathrm{d}I_{\mathrm{for}}(\lambda, I_0, z) = E_\mathrm{L}\,\beta_{\mathrm{for}}(\lambda, \lambda_0, I_0, z_{\mathrm{em}})$$
$$\times\exp\left(-\int_{z_{\mathrm{em}}}^{z}\alpha_\ell(\lambda, z')\mathrm{d}z'\right) T_{\mathrm{NL}}(\lambda, I_0, z_{\mathrm{em}})\mathrm{d}z_{\mathrm{em}}\,. \tag{15}$$

Of course, both processes described above occur simultaneously so that their contributions add, which leads to

$$E(\lambda, I_0, z) = E_\mathrm{L}\frac{A_0}{z^2}\frac{c\tau_\mathrm{d}}{2}\exp\left(-\int_0^z \alpha_\ell(\lambda, z')\mathrm{d}z'\right)$$
$$\times\left\{\xi_{\mathrm{NL}}(\lambda, I_0, z)\beta_{\mathrm{back}}(\lambda, \lambda_0, I_0, z) + \pi(\theta_{\mathrm{CE}})^2\beta(\lambda_0, I_0, z)\right.$$
$$\times\int_0^z\left[\xi_{\mathrm{NL}}(\lambda, I_0, z_{\mathrm{em}}, z)\beta_{\mathrm{for}}(\lambda, \lambda_0, I_0, z_{\mathrm{em}})\right.$$
$$\left.\left.\times\exp\left(-\int_{z_{\mathrm{em}}}^{z}\alpha_\ell(\lambda, \varrho)\mathrm{d}\varrho\right) T_{\mathrm{NL}}(\lambda_0, I_0, z_{\mathrm{em}})\right]\mathrm{d}z_{\mathrm{em}}\right\}. \tag{16}$$

Note that the signal $E(\lambda, I_0, z)$ actually represents a spectral density since $[\beta_{\mathrm{back}}] = [\beta_{\mathrm{for}}] = [\beta]/[\text{length}]$.

The determination of β_{back} and β_{for} for white-light generation as well as their angular dependence is not straightforward. Spectral broadening depends on several processes such as plasma ionisation or self-phase modulation. For this reason, the efficiency of the frequency conversion from λ_0 to λ can only be defined under strong assumptions. Moreover,

recent experimental measurements [5, 6, 25] show inconsistencies about the shape of the white-light spectrum in the visible domain. This point is beyond the scope of the paper, but it should be clarified before issuing some definite expression for β_{for} and β_{back} and obtaining a more explicit version of (16).

4 Conclusion

Gathering the results for the overlap function and the intensity attenuation, we finally find the main changes to the lidar equation implied by nonlinear propagation of high-power ultrashort laser pulses, for both mono- and multi-spectral lidar configurations. This propagation entails a modification of the geometrical factor ξ because of self-focusing and subsequent filamentation. The high intensities that are reached in the filaments also result in a strongly nonlinear extinction of the pulses, thus modifying the scattering (α) term. The changes proposed in this paper can combine with the modifications described by Kasparian et al. [4] for the backscattering (β) term. Actually, such a nonlinear lidar equation is essential for the interpretation of lidar signals from femtosecond pulses [5, 6], which could permit a more complete remote sensing of the atmosphere.

Acknowledgements. J. Kasparian acknowledges financial support of the Deutsche Forschungsgemeinschaft in the framework of the French–German project 'Teramobile' (CNRS/DFG).

References

1. R.M. Measures: *Laser remote sensing – Fundamentals and applications* (Wiley Interscience, New York 1984)
2. E. Frejafon, J. Kasparian, P. Rambaldi, B. Vezin, V. Boutou, J. Yu, M. Ulbricht, D. Weidauer, B. Ottobrini, E. de Saeger, B. Krämer, T. Leisner, P. Rairoux, L. Wöste, J.-P. Wolf: Eur. Phys. J. D **4**, 231 (1998)
3. J. Kasparian, E. Frejafon, P. Rambaldi, J. Yu, B. Vezin, J.-P. Wolf, P. Ritter, P. Viscardi: Atmos. Environment **31**, 2957 (1998)
4. J. Kasparian, J.-P. Wolf: Opt. Commun. **152**, 355 (1998)
5. P. Rairoux, H. Schillinger, S. Niedermeier, M. Rodriguez, F. Ronneberger, R. Sauerbrey, B. Stein, D. Waite, C. Wedekind, H. Wille, L. Wöste: Appl. Phys. B **71**, 573 (2000)
6. L. Wöste, C. Wedekind, H. Wille, P. Rairoux, B. Stein, S. Nikolov, Chr. Werner, S. Niedermeier, H. Schillinger, R. Sauerbrey: Laser Optoelektronik **29**, 51 (1997)
7. P.B. Corkum, C. Rolland, T. Srinivasan-Rao: Phys. Rev. Lett. **57**, 2268 (1986)
8. J. Kasparian, R. Sauerbrey, D. Mondelain, S. Niedermeier, J. Yu, J.-P. Wolf, Y.-B. André, M. Franco, B. Prade, S. Tzortzakis, A. Mysyrowicz, M. Rodriguez, H. Wille, L. Wöste: Opt. Lett. **25**, 1397 (2000)
9. A. Braun, G. Korn, X. Liu, D. Du, J. Squier, G. Mourou: Opt. Lett. **20**, 73 (1995)
10. E.T.J. Nibbering, P.F. Curley, G. Grillon, B.S. Prade, M.A. Franco, F. Salin, A. Mysyrowicz: Opt. Lett. **21**, 62 (1996)
11. A. Brodeur, C.Y. Chien, F.A. Ilkov, S.L. Chin, O.G. Koserava, V.P. Kandidov: Opt. Lett. **22**, 304 (1997)
12. M. Mlejnek, E.M. Wright, J.V. Moloney: Opt. Lett. **23**, 382 (1998)
13. B. La Fontaine, F. Vidal, Z. Jiang, C.Y. Chien, D. Comtois, A. Desparois, T.W. Johnson, J.-C. Kieffer, H. Pépin, H.P. Mercure: Phys. Plasmas **6**, 1615 (1999)
14. A. Brodeur, F.A. Ilkov, S.L. Chin: Opt. Commun. **129**, 193 (1996)
15. O.G. Kosareva, V.P. Kandidov, A. Brodeur, C.Y. Chien, S.L. Chin: Opt. Lett. **22**, 1332 (1997)
16. N. Aközbek, C.M. Bowden, A. Talebpour, S.L. Chin: Phys. Rev. E **61**, 4540 (2000)
17. Y. Silberberg: Opt. Lett. **15**, 1282 (1990)
18. E.E. Fill: J. Opt. Soc. Am. B **11**, 2241 (1994)
19. A. Chiron, B. Lamouroux, R. Lange, J.-F. Ripoche, M. Franco, B. Prade, G. Bonnaud, G. Riazuelo, A. Mysyrowicz: Eur. Phys. J. D **6**, 383 (1999)
20. S. Trillo, A.V. Buryak, Y.Z. Kivshar: Opt. Commun. **122**, 200 (1995)
21. L. Torner, J.P. Torres, C.R. Menuyuk: Opt. Lett. **21**, 462 (1996)
22. P.M. Goorjian, A. Taflove, R.M. Joseph, S.C. Hagness: IEEE J. Quantum Electron. **QE-28**, 2416 (1992)
23. V.P. Candidov, O.G. Kosareva, S.A. Shlyonov: Nonlinear Opt. **12**, 119 (1995)
24. J. Kasparian, R. Sauerbrey, S.L. Chin: Appl. Phys. B **71**, 877 (2000)
25. J.-P. Wolf, Y. Pan, G.M. Turner, M.C. Beard, C.A. Schmuttenmaer, S. Holler, R.K. Chang: Ballistic trajectories of optical wavepackets circulating within microcavities, Phys. Rev. A, in press (2001)
26. J. Yu, D. Mondelain, G. Ange, R. Volk, S. Niedermeier, J.-P. Wolf, J. Kasparian, R. Sauerbrey: Backward supercontinuum emission from filaments generated by ultrashort laser pulses in air, Opt. Lett. **26**, 533 (2001)